REPORT DOCUMENTATION PAGE

AFRL-SR-AR-TR-04-

0648

1. AGENCY USE ONLY (Leave blank)	2. REPORT DATE	3. REPORT TYPE AND DATE COVERED
	30Nov04	Final Report

4. TITLE AND SUBTITLE
Final Report:
Hadamard Transform Time-of-Flight Mass Spectrometry

5. FUNDING NUMBERS
C F49620-03-C-0074

6. AUTHOR(S)
Steve Massick

7. PERFORMING ORGANIZATION NAME(S) AND ADDRESS(ES)
Southwest Sciences, Inc
1570 Pacheco St.
Suite E-11
Santa Fe, NM 87505

8. PERFORMING ORGANIZATION REPORT NUMBER
R03-14-4

9. SPONSORING/MONITORING AGENCY NAME(S) AND ADDRESS(ES)
AFOSR/NL
Dr Michael R. Berman
4015 Wilson Blvd Room 713
Arlington VA 22203-1954

10. SPONSORING/MONITORING AGENCY REPORT NUMBER

11. SUPPLEMENTARY NOTES

12a. DISTRIBUTION/AVAILABILITY STATEMENT
Approve for Public release: Distribution Unlimited

12b. DISTRIBUTION CODE

13. ABSTRACT (*Maximum 200 Words*)

Report developed under STTR contract for topic AF03T003. This program applied the Hadamard transform method to atmospheric pressure ion mobility separation (IMS) for the analysis of trace species. Target applications include chemical and biological agent detection as well as protein sequencing and identification. We demonstrate that the Hadamard transform approach improves sensitivity by increasing sample throughput, yet requires only minimal modification to the existing hardware. In Phase I we programmed commercially available DSP electronics that operated an existing IMS for Hadamard transform modulation and collected ion signal synchronous with yet at higher rates than the Hadamard modulation sequence. This strategy allows for parsing of the analog signal to avoid noise associated with the pulsing of the Bradbury Nielson ion gate and also allowed for easy comparison of various modulation rates and sequence lengths.

14. SUBJECT TERMS	15. NUMBER OF PAGES	16. PRICE CODE
	7	

17. SECURITY CLASSIFICATION OF REPORT	18. SECURITY CLASSIFICATION OF THIS PAGE	19. SECURITY CLASSIFICATION OF ABSTRACT	20. LIMITATION OF ABSTRACT

1. Table of Contents

2. Introduction.

The combination of mass spectrometry and ion mobility spectrometry is a proven method of characterizing mixtures and detecting specific chemical compounds in complex samples via two-dimensional matrices of gas phase ion mobilities and mass to charge (m/z) ratios. Modern applications range from protein analysis to explosives detection. Coupling to time-of-flight mass spectrometers (TOFMS) are preferred since complete mass spectra are acquired rather than having to scan the m/z ratio. However, the biggest drawback to both IMS and TOFMS is the inherently low duty factor, typically several percent for each. The throughput for the combined IMS/TOFMS is consequently very low, less than one-tenth of a percent. Recently, Fourier and Hadamard transform (HT) methods have been applied to TOFMS[1,2] and Fourier transform methods to IMS[3] in order to increase the duty factor. This increased throughput is important for the analysis of small biological samples and for the detection of ultra-trace contaminants including chemical warfare agents.

We describe in this report the implementation of the Hadamard transform technique to an existing atmospheric pressure IMS with minimal physical changes to an existing instrument in the laboratories of Herbert Hill at Washington State University. Comparisons are made between IM spectra obtained using both standard single pulse IMS and Hadamard transform IMS for samples of amphetamine and cytochrome C .

3. Phase I Technical Objectives

The Phase I effort was initially designed to answer the following technical questions:

1. What are the limitations imposed by the use of an ion mobility spectrometer (IMS) as an ion source for Hadamard transform TOFMS?

2. What effects do detector non-linearities and finite dynamic range have on two-dimensional Hadamard transform TOFMS?

3. What are the likely response times, modulation requirements, and computational needs of a two-dimensional, Hadamard transform IMS-TOFMS?

The combined Phase I and Phase II programs will address the following questions:

i. What improvements in sensitivity and throughput are possible using the proposed two-dimensional HT method?

ii. What would be the performance specifications (detection limits, size, sample preparation methods, power requirements, weight, *etc.*) for commercial instruments based on the proposed technology?

iii. What would be the likely costs of laboratory and field instruments based on the proposed technology?

Several factors including a change of STTR partner from David Clemmer at Indiana University to Herb Hill at WSU, delays in Southwest Science's ability to deliver required electronics to the Hill labs, and the absence of an operating TOFMS at the Hill lab once the electronics were ready necessitated changes to the proposed work plan. Instead of applying the Hadamard type modulation to a TOFMS, the modulation was applied to an atmospheric pressure IMS instrument. These changes were discussed with the technical representative of this Phase I contract.

4. Phase I Results.

4.1 Background. Ion mobility spectroscopy is analogous to time-of-flight mass spectroscopy in that both methods provide chemical analysis information using the arrival time of ions traveling from a pulsed source to a fixed detector. The major difference is that ion mobility spectrometers operate at much higher pressures (from several torr to an atmosphere); as a result, IM spectra can be dominated by ion-molecule reaction products, drift times and resolution vary with the bath gas temperature, and ion drift times depend on the ion shape as well as its charge-to-mass ratio.

There is a wide latitude in IMS operating conditions, so it is possible to tailor the IMS parameters to meet the requirements for the HT approach. For example, the IMS resolution (defined as $t_d/\Delta t$ where t_d is the drift time and Δt is the peak width) is given by

$$\frac{t_d}{\Delta t} = \left[\frac{LEze}{16 k_B T \ln 2} \right]^{1/2}$$

where L is the length of the IMS drift region, E is the applied electric field, z is the number of charges on the ion, e is the electron charge, k_B is Boltzmann's constant, and T is the temperature. The atmospheric pressure IMS instrument used for the experiments described in this report displayed a resolution of approximately 18 for amphetamine with standard single pulse operation.

Overview of Hadamard Transform methods

Harwit and Sloan[4] provide an analogy between Hadamard transform methods and "weighing problems." They point out that weighing n objects is best performed – finding the most accurate result – by weighing the objects in combinations instead of one at a time. The number of actual measurements remains the same, but the accuracy improves by $\sqrt{n}/2$ for n items. This weighing analogy may be represented by the operation of a binary matrix upon the individual unknown weights (Ψ_n) resulting in the measurements, (η_n). Thus, in this example the square matrix

describes a series of masks (rows) that determine which weights are combined to form measurements, $\eta = S_n \Psi$. Matrices of this type may be optimized to minimize error and have been extensively studied in the field of optics[4] and signal multiplexing.[5] A particularly useful class of these matrices are the Hadamard type and the related simplex code matrices (S matrices). Hadamard transforms apply to situations in which unknown quantities may be added and subtracted to form measurements while unknown quantities that can only be added or omitted utilize S matrix transforms.

S matrices may be generated for applications involving large numbers of measurements, such as ion mobility spectra, from simple binary operations for sequence orders of $n = 2^m - 1$ where m is the length of a bit shift operation.[4] Figure 1 illustrates the series of XOR operations used to generate the maximal length pseudo random sequence (MLRPS)or row of a S matrix of order $n = 255$. Subsequent rows are formed by rotating the entire modulation sequence by the row index to form a square matrix of order 255, S_{255}. For the experiments described below, the typical length of the shift operations is 13 resulting in S matrices of order 8191. These patterns were output at rates of ~ 3 to 20 kHz, modulation periods ranged from 50 μs to 300 μs.

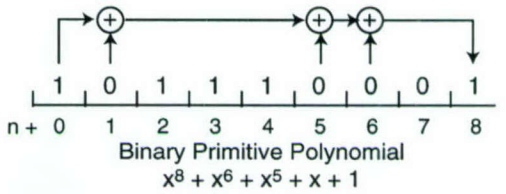

Figure 1 Illustration of the binary operations for the generation of a 255 element pseudorandom sequence.

4.2 Pulse Sequence and Data Collection Electronics. Digital signal processing (DSP) electronics from SignalWare and Spectrum Digital were used for the output of Hadamard type sequences and data collection. The programming of a SignalWare AED-101 A/D and D/A board and DSK6713 controller board combination is written in C using the Code Composer Studio development environment. The program fulfills the requirements for this project, i.e. it operates the AED-101 to output multiple long modulation pulse sequences and to synchronously collect input signals.

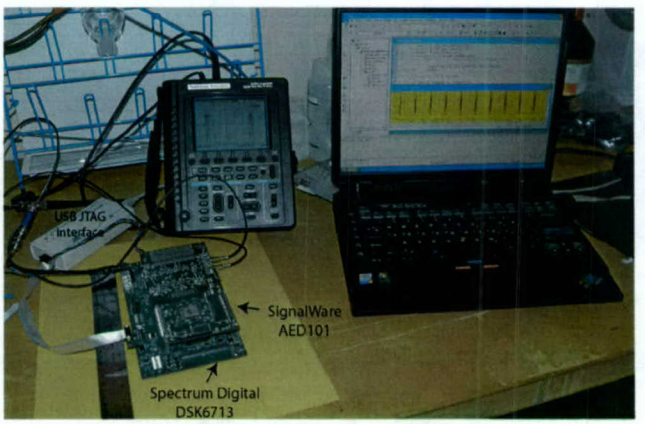

Figure 2 Phase I DSP control electronics.

The AED-101 is capable of short bursts of analogue to digital (A/D) acquisitions at 90 MHz, the clock rate of the external memory interface (EMIF) on the DSK6713. However, the effective data transfer rate from the AED-101 to memory on the DSK6713 limits A/D conversion rate to 45 MHz (EMIF/2). Furthermore, the need to continuously output a series of Hadamard sequences that are larger than the D/A FIFO buffer on the AED-101 board requires refreshing the D/A FIFO by transfers from the DSK6713 to the AED101. Simultaneous operation of both the A/D and D/A limits the A/D acquisition rate to 30 MHz with a D/A output rate of 15 MHz. Note

that we acquire data at twice the rate of the modulation sequence. The details of the hardware and programming are described in detail below.

AED-101 modifications.

The AED-101 board has two A/D channels, two D/A channels, and 16 digital input/output lines (DIO). Although it would be possible to output modulation sequences on the DIO lines, these outputs are unbuffered and would require constant time-critical writes that would cripple the signal data transfer from the A/D converter. Instead, we chose to request from SignalWare modifications to the field programmable gate array (FPGA) on the AED-101 that would compress the D/A data to effectively convert the D/A output to DIO lines. The modifications are illustrated in Figure 3. The FPGA orchestrates the activity of the AED101 by controlling both the A/D and D/A FIFO buffers (32 bit x 511 element), dividing the EMIF clock to generate synchronous output and input clocks, generating triggers to initiate enhanced direct memory addressing (EDMA) A/D data transfers and to count D/A conversions on a DSK6713 timer pin (TINP1), and, most importantly, packing and unpacking 32 bit data elements in the FIFO's according to the specified resolution for the A/D and D/A, respectively. EDMA data transfers occur mostly independent of central processor (CPU) activity and are critical to high speed operation of the AED101 with simultaneous background data processing. SignalWare modified the FPGA program to interpret the 32 bit D/A FIFO data elements as two 16 bit values for each of the two D/A channels. Each 16 bit value is then interpreted as 16 x one bit values, thereby compressing the D/A data sixteen-fold by reducing the resolution of the D/A. A zero value is interpreted as full scale negative output of the D/A, and a value of one as full scale positive output. This sixteen fold reduction in D/A data transfer size minimizes both the memory and transfer time requirements. In addition, we requested an FPGA that operates only one of the A/D converters at a resolution reduced from 12 bits to 8 bits. The FPGA then combines four 8 bit A/D samples into each 32 bit EDMA transfer element, resulting in a four-fold compression of the A/D data.

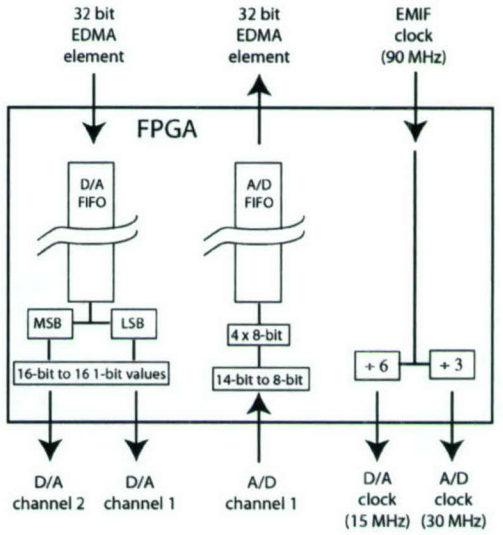

Figure 3 AED101 FPGA block diagram.

AED-101 programming and testing.

A sample C program written for Code Composer provided by SignalWare compiled and executed as specified with slight modifications to accommodate our non-standard FPGA configuration. This program was useful primarily to demonstrate that the FPGA was operating correctly. We confirmed the format of both the A/D and D/A 32-bit word transfers to the respective FIFO's. Otherwise, the subroutines were found to be of limited utility since these had been written for older Texas Instrument DSP processors as well as older versions of Code

Composer and did not operate the A/D and the D/A channels simultaneously. Also, EDMA data transfer was used only for A/D data transfers with D/A values assigned by CPU assignment statements.

We first tested EDMA transfers to the D/A FIFO without running the A/D converter. There are two distinct fields in the AED FPGA control register that allow starting either the D/A or A/D converters. Our test program executed the following steps. The D/A FIFO was initialized with an easily recognizable pattern constructed by repeating four 16 bit integers with values 0x0FF5, 0xFFF0, 0xFF00, and 0x500F. One of the timers on the DSK6713 board was configured to use the D/A 'conversion pulses' produced by the AED101 FPGA as the clock input. This timer was linked to initiate EDMA transfers to the D/A FIFO from internal RAM on the 6713 CPU. For this test the D/A EDMA channel parameters are linked to the first of four EDMA parameter table entries that contain the IRAM addresses of a cyclic buffer with four memory regions. The IRAM buffer contains a larger sequence of the same pattern as that of the D/A FIFO. The FPGA interprets each 16 bit FIFO value starting at the least significant bit. Consequently, the pattern observed on the oscilloscope upon execution was ...AFF00FFF00FFF00A..., continuously. To our surprise, we discovered that the AED FPGA produced a 'conversion pulse' for every value taken off of the D/A FIFO buffer rather than for every update of the D/A output. Thereby, one pulse is generated for every sixteen D/A conversions. This prevents us from counting TINP1 pulses to initiate a software interrupt at the end of the modulation sequences since the length of these sequences are necessarily odd, 2^n-1 where n is the bit shift. It will be easy to correct this inconvenience in future versions of the FPGA program. After adding a correction to the number of pulses counted prior to each EDMA transfer, a digital storage oscilloscope was used to check the D/A output. The test pattern was displayed without any FIFO under flows or other glitches.

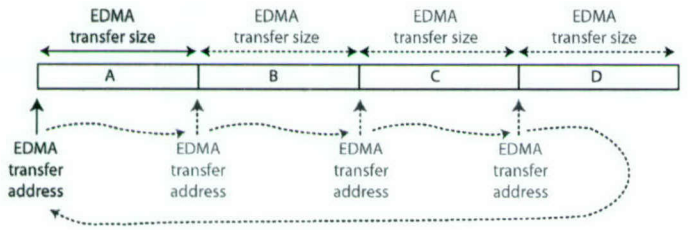

Figure 4 Illustration of the EDMA four segment buffer used for testing continuous D/A output of the AED101.

Our next test program was designed to evaluate simultaneous D/A and A/D operation of the AED101. The same test pattern and method of counting the TINP1 pulses to trigger EDMA refreshes of the D/A FIFO as described above was used and a second EDMA channel was configured to capture 1024 A/D values per EDMA transfer to a similar four segment cyclic buffer residing in IRAM. The FPGA on the AED101 board was configured to trigger A/D EDMA transfers from the A/D FIFO when the A/D FIFO was 96% full. The A/D EDMA

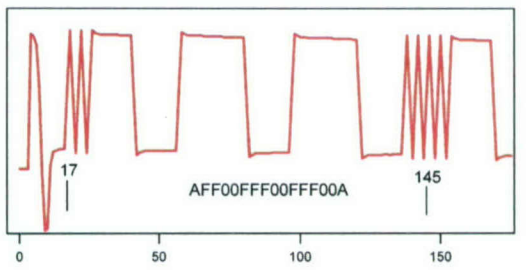

Figure 5 Test pattern output by D/A converter, collected by A/D converter on AED101.

transfer was also configured to initiate a hardware interrupt that counted the number of transfers and set a flag to indicate that valid data was available in the current IRAM segment. For this test the D/A output was connected to the A/D input, the A/D and D/A clock rates were 10 MHz and 5 MHz, resp., and the program was terminated after 4 EDMA transfers. Figure 5 is a plot of the D/A output captured by the A/D immediately following simultaneous start of the D/A and A/D. The pattern is output and collected correctly without any pauses for EDMA data transfers. It is interesting that the first 17 A/D values are always not related to the pattern we load in the D/A FIFO and appear to be related to a flaw in the D/A portion of the FPGA program. This is not a serious problem and will likely result in only a offset correction.

The data transfer strategy detailed above uses two independent EDMA channels, each receiving separate triggers with the D/A EDMA transfer assigned a lower priority than the A/D transfer. The rational for this choice is that the highly compressed D/A data has lower transfer time requirements, the D/A is run at half the clock speed of the A/D, and interrupting transfers from the A/D FIFO is likely to cause FIFO overflows and loss of data. Attempts to increase the A/D clock rate above 10 MHz using this strategy results in erratic outputs related to D/A FIFO underflows. We tried playing tricks such as varying the D/A refresh size to synchronize the timing of the A/D and D/A EDMA events and varying the priorities of the two EDMA transfers. We were unable to operate clock rates higher than 10 MHz using independently triggered EDMA channels.

We tested a second EDMA strategy to run the A/D and D/A operations continuously at 30 MHz and 15 MHz, respectively. This strategy uses only the A/D FIFO full trigger from the AED101 for the timing of the A/D and D/A data transfers. The EDMA transfer to the D/A FIFO buffer is triggered by the completion of the A/D EDMA transfer. Linking the two EDMA channels in this manner prevents any interference as long as the smaller D/A transfer is complete before the A/D FIFO fills and triggers the next A/D EDMA transfer.

The A/D data once transferred to the DSK6713 requires processing for both averaging the signals of the appropriate lengths according the applied modulation and transforming the averaged signal to ultimately extract the TOF mass spectrum. The 64 bit test pattern described above was again used, however, for purpose of programming a data averaging subroutine we allocated more memory for the D/A pattern storage. Stored in this memory segment are mock modulation sequences composed of the 64 bit pattern $2^9 - 1$ repeated to form a 511 bit sequence where the last bit of the last 64 bit pattern is omitted. The complete D/A output pattern consisted of 24 modulation of these sequences. Since the D/A data is compressed sixteen-fold the memory requirements were minimal, still smaller than the four segment A/D signal memory buffer. The mock modulation sequence length of 511 corresponds to 1022 A/D values just less than the EDMA transfer size of 1024 8-bit values. We attempted to accumulate an average by adding the elements of the most recent A/D buffer segment to an array then waiting for the second A/D segment to fill, and so forth. The averaging subroutine failed to keep pace with the data collection, therefore EDMA transfers to the circular A/D buffer would overwrite data before that data was added to the sum. Although operation of the 6713 CPU at 225 MHz should be more

than adequate to perform the summation, the overhead arising from conditional statements to recognize the pattern start and stop positions in the buffer segment, hardware interrupt initiation and return, and updating the D/A address position for the EDMA is sufficiently large to slow the effective summation speed to less than the 30 MHz acquisition rate.

The idea of using a circular buffer for the A/D acquisitions was abandoned and replaced with storing all the A/D and D/A data in the 8 megabyte external SDRAM on the DSK6713. The IRAM memory size is only 192 kilobytes, too small for complete A/D data sets that will be on the order of one megabyte. We did not initially try this because memory access is slower for EDMA transfers to SDRAM. After incorporating new EDMA timing parameters for SDRAM transfers into the program, we discovered that we could still operate at A/D and D/A rates of 30 MHz and 15 MHz, as before. Figure 6 displays the average of 128 test pattern sequences simulating an 11 bit Hadamard sequence with the first and last pattern shown on the top and bottom plots. The entire A/D buffer of 128 x 4094 values did not contain any errors or shifts in the ..AFF00FFF00FFF00A... pattern and the calculated average of Fig. 6 shows sharp patterns un-blurred by jitter between the A/D and D/A channels. Note that the end of the sequence is missing one bit, the 0 bit of the final A hexadecimal character. This is expected for the odd sequence lengths.

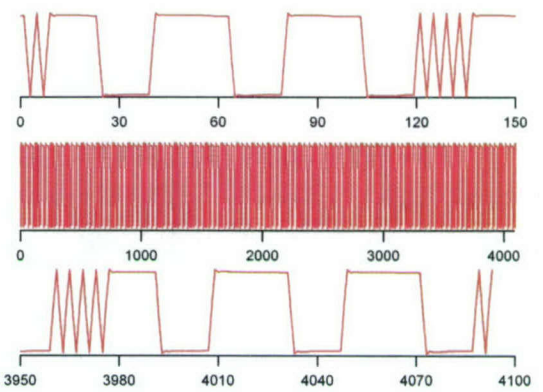

Figure 6 Average of 128 A/D collections of 2047 value test patterns output by the D/A at 1/2 the A/D clock rate.

The program can output *S* sequences are of lengths 255 to 65,535 corresponding to XOR bit shifts of 8 to 16 as described in section 4.1. Notably, we initialize the array according to Harwit and Sloane by setting the first nbit-1 values are set to zero and nbit value is set to 1, where nbit is

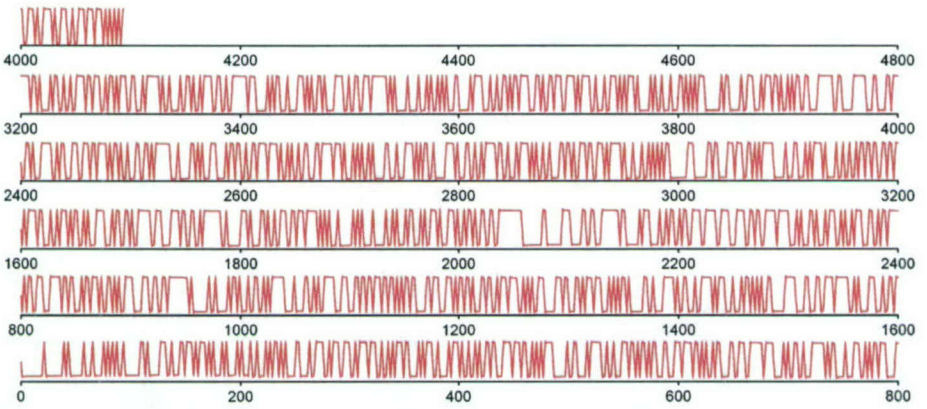

Figure 7 Average of 128 Eleven bit simplex code sequences generated and collected by the Phase I control electronics.

the value of the maximum bit shift of the XOR operations. This initialization was used for calculating the pulse sequence shown in Fig. 7. average of 128 x 11-bit (S_{2047}) simplex code sequences output at 15 MHz and sampled by the A/D at 30 MHz.

4.3 HT-IMS Results. The Phase I electronics were adequate to operate a TOFMS at reduced resolution, i.e. with peak widths of 200 ns or greater. Given that a TOFMS was not available for use in the latter part of the Phase I period, the modulation rate was reduced from 15 MHz to approximately 10 kHz to for the operation of the Hill laboratory IMS with HT modulation.

The Hill atmospheric pressure ion mobility spectrometer consists of a stack of stainless steel guard rings (47 mm I.D.), which were separated and insulated from each other by alumina rings and connected in series by resistors. The potential drop applied across this 14.1 cm drift region was 7.6 kV and the ion gate at the entrance to the drift region is a Bradbury-Nielson gate. Nitrogen gas was flowed counter-current to the ion drift velocity at 800 ml/min. For these experiments, ion signal collected by Faraday plate at the exit of the drift region was amplified by a Keithley 427 current amplifier with a gain setting of 10^8 and 30 μs time constant for all spectra reported below. For the HT-IMS implementation, the output of the Keithley 427 was sampled by the A/D converter of the SignalWare AED-101. Otherwise, standard IM spectra were collected by a LabView E-series DAQ card.

The Bradbury-Nielson gate admits ions into the drift region by pulsing off a 80 V potential difference applied between the two wire grids of the gate. The gate is floated at 7.6 kV and a custom built pulsing circuit is triggered by logic pulses either from the AED-101 for HT-IMS or by a digital line from the LabView DAQ card for standard IMS operation. An electrospray ionization (ESI) source consisting of 75 μm I.D. polyimide tubing was held 4 to 5 cm from the gate and floated at 11.6 kV. A syringe pump controlled the sample flow to typically 3 μl/min. The solvent for sample preparation was 25% methanol and 1% acetic acid in water.

For these preliminary experiments raw data from the DSP electronics was transferred to a personal computer. This rather slow process allowed us to evaluate different methods of processing the data prior to performing the inverse transform. The DSK6713 is capable of performing the inverse transform and this would be the preferred mode of operation since it would greatly reduce the amount of data transferred from the DSK6713. For example, a typical length for the raw data is over 8000. Transformed to a 25 ms ion drift spectrum the length is reduced to less than 200.

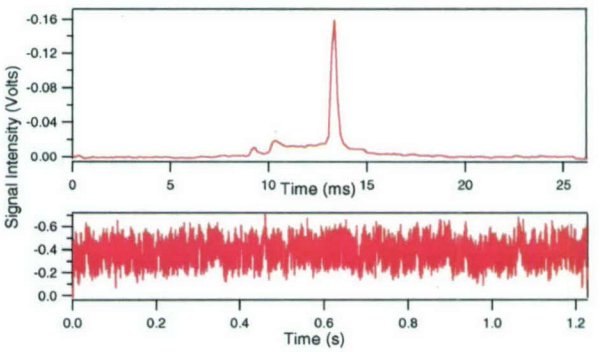

Figure 8 HT-IMS raw data and inverse transform for amphetamine (20 ppm).

4.3.1 Amphetamine. All of the amphetamine experiments were performed with 20 ppm sample concentrations. Figure 8 displays in the lower plot the raw data from an HT-IMS experiment, in this case a signal average for two complete $\boldsymbol{S}_{8191}$ patterns, and the ion drift spectrum retrieved for a 25 ms window in the upper plot. The pulse width of the modulation is 150 μs and the total sampling time is 2 x (8191 x 150 μs) or a total of 2.46 seconds. Two solvent peaks are noticeable near 10 ms and amphetamine is seen as a well-resolved peak at 13.4 ms.

As noted before, the ion signal is sampled at twice the rate of the modulation and we have evaluated different methods of treating the raw data prior to performing the inverse transform. We expected that noise associated with the pulsing of the Bradbury-Nielson gate would appear on the signal. Consequently, our initial method used to process the data was to parse the raw data by selecting only the A/D points that do not coincide with the D/A clock, i.e. the modulation clock. We effectively throw half the data away. Ion mobility drift spectra calculated from the same 150 μs $\boldsymbol{S}_{8191}$ raw data as in Figure 8 using several methods of data treatment are shown in Figure 9. Transforming all data with a doubled $\boldsymbol{S}_{8191}$ pattern (top trace) results in noisy baselines that makes the identification of small peaks difficult and is the worst of the four methods. Averaging the A/D points closest to the gate pulses with those furthest from the gate pulses reduces the noise in the baseline but displays an odd peak shape for amphetamine as well as a much higher peak height. Lastly, it is interesting that selecting only the points closest to the gate pulses (bottom trace) does not result in a noisy baseline indicating that the gate noise is quite consistent. However, the peaks retrieved in this manner are reduced in height and broad. The best method and the only one that does not exhibit a glitch near zero milliseconds is parsing the raw data by selecting only the points that do not coincide with the modulation clock. It should be possible to take advantage of the slower IMS time scales and sample the ion signal at even higher rates than twice the modulation rate. Thereby, benefitting from taking an average all points except those closest to the modulation clock and further improving the S/N ratio. This was not attempted in Phase I.

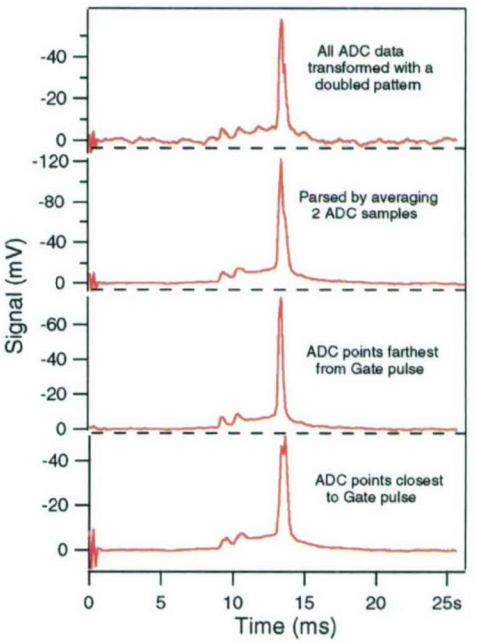

Figure 9 Comparison of different methods of HT-IMS data treatment.

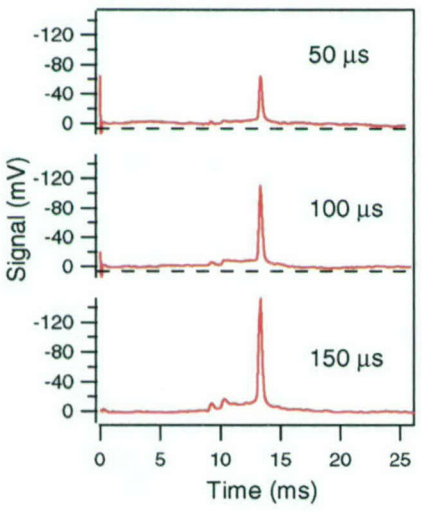

Figure 10 HT-IM spectra for various modulation periods

The Hill laboratory typically operates the Bradbury-Nielson gate of the IMS instrument by applying at least a 300 μs wide pulse to admit ions to the drift region. Shorter

gate pulse widths attenuate the signal and give poor results. For HT-IMS operation, the modulation rate defines the minimum gate width and the time resolution of the drift spectra obtained. Considering that the full width half maximum (FWHM) peak widths obtained for standard single pulse IMS are 400 μs, time resolutions of 300 μs are not desirable. We evaluated the effects of short pulse widths, i.e. high modulation rates on HT-IM spectra. The spectra acquired with 50, 100, and 150 μs modulation periods are shown in Figure 10. The signal to noise ratio improves with longer modulation periods with no significant loss in resolution. Attempts to increase ion throughput at the short gate widths by increasing the electric field before the Bradbury Nielson gate did not result in any significant improvements. The 150 μs modulation period gave the best results and this was used for the remainder of the studies.

The length of the bit shift operation used to generate the maximal length pseudo random sequence (MLRPS) (a row of the S matrix) determines several important aspects of HT-IMS. Firstly, it dictates the minimum acquisition time for acquisition of an HT-IMS drift spectrum. For example, a 13 bit XOR operation results in a modulation pattern 8191 elements long. If the modulation period is 150 μs, then the acquisition time for one full pattern is 1.23 seconds. Secondly, the quality of data is expected to increase with increasing bit shift lengths. This is due to a characteristic of the MLRPS's that the longest pulse period for a sequence generated by a bit shift equal to *m* is *m* modulation periods and the longest off period is *m*-1 periods. One way of thinking of this is that the longer MLRPS's have a greater depth of modulation. Shown in Figure 11 are HT-IM spectra acquired using MLRPS's generated by bit shift operations ranging from 10 to 13, i.e. minimum acquisition times from 150 ms to 1.23 seconds. The drift spectra are averages of 256 patterns for the 10 and 11 bit spectra and 128 patterns for the 12 and 13 bit spectra. The difference in noise is not due to differences in acquisition times as the 10 bit spectrum corresponds to a 20 second acquisition time and shows no improvement with additional signal averaging. Also, initially the second full pattern contains valid data since in order for the transform to be valid there must be overlap of data from the modulation applied by the first pattern. The loss of the first patterns data upon startup is not an important concern since in most implementations of HT-IMS the modulation will be run continuously.

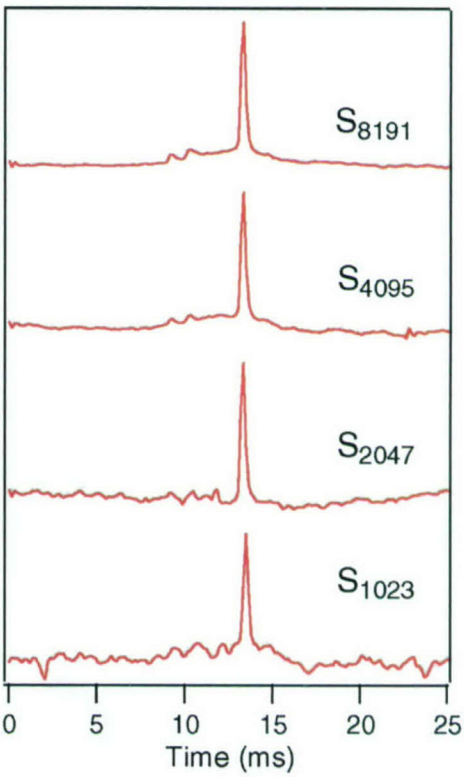

Figure 11 Comparison HT-IMS results at various modulation sequence lengths.

We observed improved signal to noise ratios for the HT-IMS data for acquisition times ofseveral seconds. Shown in Figure 12 is a comparison of drift spectra for 20 ppm amphetamine for standard single pulse IMS taken with a 300 μs wide pulse applied to the Bradbury-Nielson gate and for HT-IMS taken with a S_{8191} sequence and a 150 μs modulation period. All other experimental conditions are identical. The HT -IMS spectrum clearly displays solvent peaks centered about 10 ms and a broad feature from 8 to 17 ms as well as the strong amphetamine peak at 13.4 ms. The standard IMS spectrum of amphetamine also shows these three weaker features with longer sampling times. Although, at 2.46 second acquisition time the weaker features are not clearly distinguishable from the baseline noise in the standard IMS drift spectrum. We quantify the signal to noise ratio as peak height divided by the standard deviation of the baseline region between 20 and 25 ms. This baseline region is clear of signal at longer acquisition times. Using this method the calculated signal to noise ratios are 315 for the HT-IMS data and 97 for the standard IMS, both with 2.46 s acquisition times.

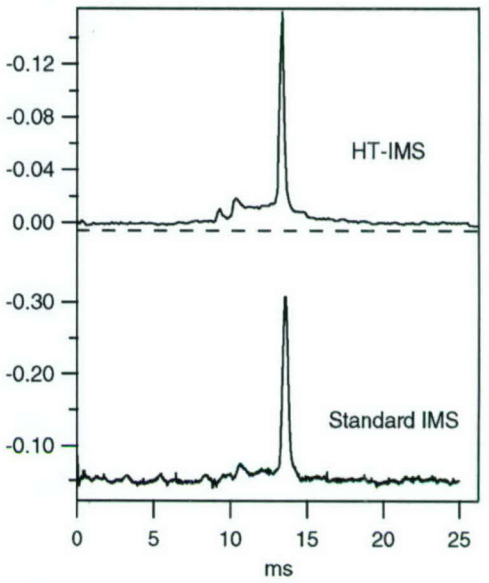

Figure 12 Comparison of amphetamine signals for 2.46 acquisition times

The signal to noise ratios of the HT-IM spectra do not significantly improve for averages over 2 patterns. The standard IMS achieves a signal to noise ratio equivalent to the HT-IMS at 10 second acquisition times and continues to improve with more averaging. Figure 13 illustrates this point. That the HT-IMS and the standard IMS do not approach the same asymptotic signal to noise ratio is likely due to the difference in resolution of the A/D data between the two methods. The standard IMS setup uses an E-series LabView DAQ card with a 12 bit analogue to digital converter (ADC). The SignalWare AED 101 ADC is a 12 bit converter, however, in the interest of optimizing data transfer speeds only the most significant 8 bits of the ADC are transferred. This reduction of resolution for data transfer speed is critical for the fast time scales typical of TOFMS and is not necessary for the slower time scale of IMS. It would only require reprogramming by SignalWare of the AED101 FPGA to restore transfers of the full 12 bits. With this accomplished, we expect that the HT-IMS data would then display the

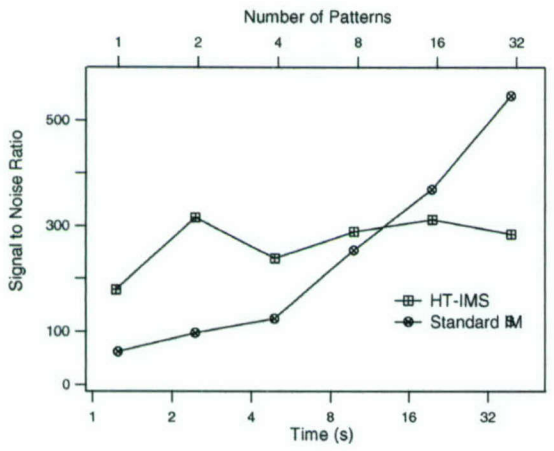

Figure 13 Signal to noise ratio comparison for amphetamine, 20 ppm, 3 μl/min.

same asymptotic signal to noise ratio as the standard IMS data. However, it would reach this asymptote much faster which would give the HT-IMS technique a clear advantage in response time and detection limits when coupled to another separation technique such as HPLC.

Direct comparisons of the resolution of the HT-IM spectra to the standard technique is complicated by the different pulse widths applied to the Bradbury Nielson Gate. Using a 150 μs gate width for the standard IMS collection will result in at least equivalent resolving power for the strong amphetamine peak than that of HT-IMS but at the expense of over half the signal to noise ratio. Rather, we choose to make resolving power comparisons between HT-IMS and standard IMS for Bradbury Nielson gate widths appropriate for the technique, that is 150 μs for HT-MS and 300 μs for standard IMS. The results are shown in Figure 14.

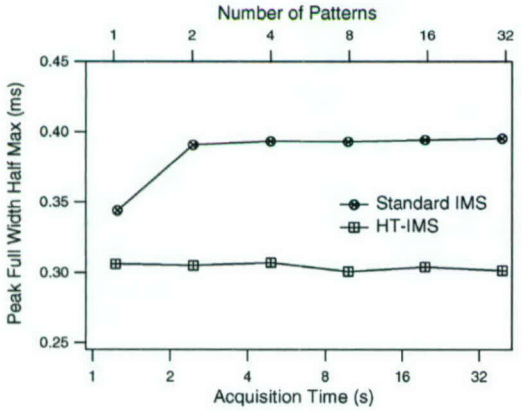

Figure 14 Comparison of amphetamine IMS peak widths.

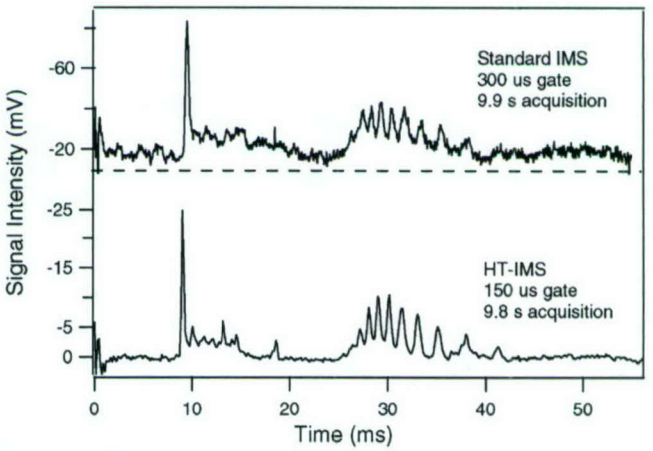

Figure 15 Comparison of cytochrome C.

We chose to measure cytochrome C with HT-IMS to evaluate the effects of congested spectra and longer ion drift times. A 100 μM cytochrome C in 25% methanol, 1% acetic acid water solution was freshly prepared for these experiments. The sample flow rate was 3 μl/min. The Bradbury Nielson (B-N) gate pulse widths were 300 ms for the standard IMS and 150 ms for the HT-IMS with a $\boldsymbol{S}_{32767}$ (15 bit) modulation. Shown in Figure 15 is a comparison of HT-IMS and standard IMS results for cytochrome C measurements. The HT-IMS cytochrome C drift spectrum displayed the two small shoulders at 26 to 27 ms that were apparent only after extensive signal averaging with the standard IMS collection. Also, the extended timescale necessary for the longer drift times of cyctochrome C illustrates an important difference between the two IMS operation methods. Extending the time window for the standard IMS requires slowing the collection rate resulting in less signal averaging for a given acquisition time, e.g. less than half as many B-N gate pulses are averaged for cytochrome C than would be for amphetamine drift spectra. Whereas the amphetamine results indicated equivalent signal to noise ratios at 10 second acquisition times, it is clearly not the case for the for the cytochrome C measurements. The cytochrome C HT-IMS data is an average of two modulation patterns each taking 4.9 seconds and, if desired, can be transformed to display the drift spectra for the full

pattern length.

5. Key Research Accomplishments.

- First demonstration of Hadamard transform ion mobility separation.
- Use of compact, low-power digital signal processing electronics for implementation of HT-IMS.
- HT-IMS displays improvements in signal to noise and resolution.

6. Reportable Outcomes.

We are in the process of writing a HT-IMS paper for submission to Analytical Chemistry.

7. Conclusions.

Our results from the Phase I research indicate that substantial benefits are possible by applying a Hadamard type modulation to ion mobility separations. The advantages of HT-IMS include better signal to noise ratios (SNR) and improved resolution associated with the narrower Bradbury-Nielson gate widths used for HT-IMS. We are confident that operation of a HT-IMS coupled to a TOFMS is possible where multiple mass channels can be monitored and each channel transformed to retrieve a matrix of ion mobilities and mass to charge ratios. The use of the TOFMS as the detector for the HT-IMS should isolate the ion signal from the B-N gate noise and lead to greater improvements to the SNR. Furthermore, the enhanced SNR of the HT-IMS method, and improved response times, is expected to increase the effectiveness of chromatographic separations applied prior to the HT-IMS.

8. References.

1. Brock, A., N. Rodriguez, and R.N. Zare, *Characterization of a Hadamard transform time-of- flight mass spectrometer.* Rev. Sci. Instr., 1999. **71**(3): p. 1306-1318.
2. Brock, A., N. Rodriguez, and R.N. Zare, *Hadamard Transform Time-of-Flight Mass Spectrometry.* Anal. Chem., 1999. **70**: p. 3735-3741.
3. Y. H. Chen, W. F. Siems, and H. H. Hill, Jr., *Fourier Transform Electrospray Ion Mobility Spectrometry*, Analytica Chimica Acta, 1996., **334**: p. 75-84
4. Harwit, M. and N.J.A. Sloane, *Hadamard Transform Optics*. 1979, New York: Academic Press.
5. Porat, B.., *A Course in Digital Signal Processing*. 1997 New York: John Wiley and Sons.